Visual Abstract

Fracture toughness of matrix cracked FRC and FGC beams using equivalent TPFM

A.A. Elakhras, M.H. Seleem, H.E.M. Sallam
Materials Engineering Department, Faculty of Engineering, Zagazig University, Zagazig 44519, Egypt
ahmedali.elakhras@gmail.com,http://orcid.org/0000-0002-3821-1327
mhseleem1963@gmail.com, http://orcid.org/0000-0002-5777-4651
hem_sallam@yahoo.com, http://orcid.org/0000-0001-9217-9957

ABSTRACT. In the present work, the fracture toughness (K_{IC}) of full-depth (FD) fiber-reinforced concrete (FRC) and layered functionally graded concrete (FGC) matrix cracked (MC) beams has been determined by the equivalent relationships of the two-parameter fracture model (ETPFM). Forty-eight MC-FGC and MC-FD FRC beam specimens with span-depth ratios (L/d) equal 4, 5, and 6 were tested under the 3PB configuration. The MC length-depth ratio (a_o/d) remained constant equal to one-third. All FRC beams have the same hooked-end steel fibers volume fraction of 1%. The FGC beams are composed of three equal layers, i.e., FRC in the bottom layer at the tension side, normal strength concrete (NSC) at the middle layer, and high strength concrete at the upper layer in the compression side. The results showed that the predicted values of K_{IC}obtained from ETPFM are considered appropriate according to the maximum size of the non-damaged defect concept. The crack mouth opening displacement estimated from ETPFM showed acceptable values close to the present experimental results. The K_{IC} values calculated within the presence of fibers in front of and through the MC for FRC beam specimens having 1% SFs is more than twice the value of NSC.

KEYWORDS. Fiber-reinforced concrete; Functionally graded concrete; Matrix cracked beams; Equivalent TPFM; Fracture toughness.

OPEN ACCESS

Citation: Elakhras, A., Seleem, M., Sallam, H.., Fracture toughness of matrix cracked FRC and FGC beams using equivalent TPFM, Frattura ed Integrità Strutturale, 60 (2022) 73-88.

Received: 23.11.2021
Accepted: 22.01.2022
Online first: 27.01.2022
Published: 01.04.2022

INTRODUCTION

Full-depth (FD) fiber-reinforced concrete (FRC) is conventional concrete with suitable discontinuous fibers added to achieve a composite with a desirable performance level. It became known that FRC improved the particular properties of concrete despite its manufacturing cost [1]. Recently, functionally graded concrete (FGC) is a new layered composite used to achieve the favorite serviceable requests of a structural element without major influence on its performance while reducing its materials cost[2,3]. Nowadays, increasing demand is placed on FRC and FGCforrepairing construction, especially in infrastructure pavement such as rigid pavement systems constructed at airports, local streets,

ports,high-volume traffic corridors, and parking lots as in the USA [4] and Europe [2]. Most of the researchers concerned about studying FGC according to its mechanical properties conduced that FGC is more efficient than FD FRC[5–13].
However, the fracture behavior of FD FRC and FGC is still limed or not obviously according to fracture mechanics concepts. Fracture parameters of concrete are substantial properties used in concrete structures. Linear elastic fracture mechanics (LEFM) is the fundamental basis of most models. According to linear elastic fracture mechanics (LEFM), fracture energy (G_{IC})and fracture toughness (K_{IC}) are not variant with the depth of notch and the size of the beam. Thus, they are considered as material properties. Also, LEFM assumes a perfect bond between the fiber and the matrix. However, several researches reported that the K_{IC} value evaluated for notched concrete specimens using LEFM showed significant variance with different sizes and notch depth. Latterly most researches implicitly these variances by the inelastic interface response during crack growth in concrete. This inelastic response during crack growth paid attention to the role of aggregate particles in crack arresting [14–16] and the fibers in crack bridging. One of the significant problems for calculating FRC fracture parameters is substantial nonlinearity before the maximum load. Unless this stable crack extension is included in the calculations of K_{IC}, one cannot obtain a correct value of the fracture toughness of concrete. Also, fibers' presence into cracked beams from normal concrete causes the maximum loads and the fracture energy to increase dramatically [17]. Moreover, Bažant et al. [18] reported that much of the scatter in total fracture energy (G_F) calculations come from inherent randomness in the tail end of the load-crack mouth opening displacement (P-CMOD) curve and uncertainty in extrapolating the tail end of the curve to zero loads beside sources of energy dissipation [18]. In addition, the examinations of fractured specimens of FRC take place primarily due to fiber pullout or deboning and increase the fracture toughness.
Thus, numerous nonlinear fracture models have been suggested to describe brittle materials failure [19–23]. Hillerborg proposed the fictitious crack model representing the inelastic interface response during crack growth characterized by a nonlinear stress-crack displacement relationship [19]. This approach is based on predicting the macroscopic stress-crack-width relations by the softening behavior of concrete. However, According to Jenq and Shah [24], the fracture mechanism for FRC can be divided into several stages. The first stage is subcritical crack growth in the matrix and the beginning of the fiber bridging effect, where the linear elastic behavior of the composite is controlled. The second stage is the post-critical crack growth in the matrix, where there is steady-state crack growth due to the applied load and the fiber bridging stresses, and the stress intensity factor remains constant. The final stage is the resistance to crack separation, provided exclusively by the fibers pullout mechanism. According to Jenq and Shah [24], crack growth occurs when the stress intensity factor, K_{IC}, and the crack tip opening displacement (CTOD) reach a critical value.
Thus, another nonlinear model considered the elastic effective crack approach, based on the equivalent LEFM and Griffith-lrwin energy dissipation concept were proposed such as; the two-parameter fracture model (TPFM) by Jenq and Shah [21]and the size effect law (SEL) by Bažant[22]. These nonlinear fracture models presented at least two fracture parameters material. These parameters are dependent only on the fracture properties of the material, irrespective of the size and geometry of the structure. These parameters are expected to describe the failure of a concrete member. Hillerborg et al. [19]proposed the fictitious crack model to measure the total material energy of fracture($G_{F)}$. The general idea of this type of test is to measure the amount of energy absorbed when the specimen is broken into two halves [25]. Jenq and Shah proposed a TPFM and considered its two parameters; K_{IC} and the critical crack tip opening displacement CTODc are constant material properties[21]. Also, SEL for notched beams (SEL, Type-II) proposed by Bažant considered two material parameters, the critical energy release rate (G_f) and the critical effective crack extension (C_f). Since both TPFM and SEL are based on the same elastic effective crack approach, Ouyang et al. [26] suggested relationships to calculate the equivalent parameters of TPFM based on this equivalency and derived it by comparing the results with SEL. Also, other researchers are concerned with determining K_{IC} for FRC and FGM [2,5,27–29].
All these models calculated fracture parameters using a three-point bending (3PB) test on through-thickness cracked beams for concrete. However, fibers must cross the two surfaces of the pre-cracked beams to have actual field conditions and correct simulations in the actual field simulation of FRC or FGC beams. It was considered one of the difficult laboratory problems. Recently, Sallam and co-workers [5]suggested a novel method to create a pre-matrix crack (MC), representing fibers that pass through the pre- matrix crack of the specimen to represent its bridging and closing effects. This work aims to study the equivalent relationships of TPFM (ETPFM) to calculate the FGC and FD FRC beams fracture toughness with real MC specimens. Real fracture toughness reliability expected from such ETPFM for MC-specimens was checked using the maximum size of the non-damaged defect (d_{max}) [30,31].

EXPERIMENTAL PROGRAM

Materials and mix proportions

Three mixes, including normal strength concrete (NSC), FRC, and high strength concrete (HSC), were designed for the experimental program. NSC was designed based on ACI 211.1-91 [32]. According to ACI 544.4R-88 [1], SF-FRC mixtures can be mixed and placed with conventional equipment, and procedures used from 0.5 to 1.5 Vf%. However, higher percentages of fibers (from 2 to 10 volume percent) have been used with special fiber addition techniques and placement procedures. Therefore, FRC was designed by adding 1% hooked-end SF by volume fraction to NSC. Hooked-end steel fibers (SF) were used with a length equal to 35 mm, a circular cross-section of 0.80 mm, and tensile strength of 1150 MPa. Ordinary Portland cement, grade N 42.5 with content 400 kg/m^3, was used to produce both NSC and FRC. The water/ cementitious materials ratio (W/CM) was 0.53. HSC mix was produced by cement, grade N 52.5 with a total CM of 550kg/m^3, and silica fume (Master Life SF 100) as a partial replacement of CM by 10%. Also, a superplasticizer (Master Glenium RMC 315) was used as a high range water reducer by 2.5 % from the weight of the CM. The W/CM ratio was 0.27. In all mixes, dolomite having a maximum aggregate size equals to 12.50 mm, and ordinary siliceous sand were respectively used as coarse and fine aggregates. The specific gravities of the used coarse and fine aggregates were respectively 2.61 and 2.59. For the estimation of mechanical properties of mixes, cubes 150×150×150 according to BS EN 12390–3:2009 [33]were cast for the compression test. Cylinders of 300 mm height and 150 mm diameter were used to estimate indirect tensile strength according to BS EN 12390–6:2009 [34]. All beams were removed from molds after 24 hours from casting. After de-molding, all specimens were cured in moist air for 56 days. The mix proportions of the NSC, FRC and HSC mix relative to their CM by weight and mechanical properties of the three investigated mixes are given in Tab. 1.

Mix/CM(kg/m3)	Mix proportions relative to CM by weight						Mechanical properties	
	CM	Sand	Dolomite	Silica Fume	W/CM	Super plasticizer	Compressive st., f_{cu}, MPa	Indirect tensile st., f_t, MPa
NSC/(400)	1	1.91	2.38	-	0.53	-	-	27.70
FRC/(400)	1	1.91	2.38	-	0.53	-	0.02	34.55
HSC/(550)	1	1.35	1.75	0.10	0.27	0.025	-	61.33

Table 1: Mix proportions for mixtures and their mechanical properties.

Samples preparation and casting procedures

Most of the fracture models recommended notched beams with L/d ratios in the range of 2.5 to 8 to study the variation of fracture toughness or fracture energy for various L/d ratios in this range. In TPFM, Jenq and Shah [21,24] considered the standard specimen with a span-depth ratio (L/d) of 4 and the initial notch-to-depth ratio (a_o/d) equal to 1/3. Han et al. [23]also investigated the fracture toughness for notched beams with various span-depth ratios ranging from 2 to 6. Hillerborg[25]recommended standard notched beams of various L/d ratios ranging from 4 to 8 to calculate the fracture energy according to its concept. Therefore, the following span-depth ratios, L/d = 4, 5, and 6, were analyzed in the present work. Forty-eight matrix-cracked (MC) FD FRC and FGC beams were fabricated, with constant breadth equals150 mm. The initial crack-depth ratio (a_o/d) stayed equals one-third. The investigated beams were of two patterns. The 1stpatterncomprised 24 MC specimens from FD FRC. The 2ndpattern comprised 24 MC- FGC beam specimens. Four specimens were cast for each case study to take the average. The dimensions of FGC and FRC beam specimens are illustrated in Tab. 2. Three mixtures from FRC, NSC, and HSC were designed to fabricate FGC beams at equal layers in steel molds. The bottom layer at the tension side was cast from the FRC mixture. NSC was cast at the middle layer of the beam depth. HSC was cast in the upper layer at the compression zone of the beam. The same procedures used by Othman et al.[35]in casting FGC layers were followed. In the case of the FRC mixture, SFs were sprayed randomly in a continuous manner during the final stage of concrete mixing, according to the recommendations of ACI 544.4R [1]. All specimens were moist cured for 56 days. Fig. 1 shows different beams patterns and the fibers distribution across the notch.

Real matrix crack methodology

Two mm thickness plate from foam was used to make the MC at the mid-span of the beam bottom. Two grooves were cut at two sides of the steel mold to fix the foam plate. The steel fibers were permitted to cross the thin foam plate uniformly distributed. The amount of steel fibers allowed to cross the plate was assumed to be one-third of the total amount representing 1% of the concrete volume fraction. Thus, the orientation factor efficiency was 0.33 for fibers distributions for ideal theoretical assumptions in this study. Many experimental and numerical studies reported orientation factors in the range of 40-60% [36–38]. Sallam and co-workers describe the procedures of real MC in detail [5], as shown in Fig. 2.

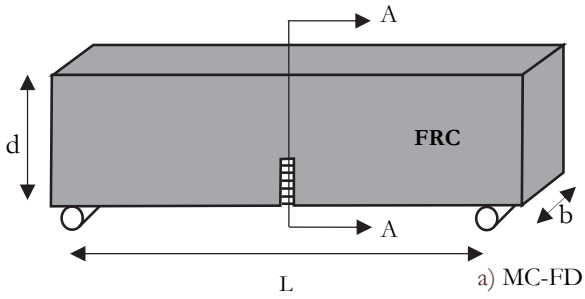

a) MC-FD FRC pattern

Cross section: A-A

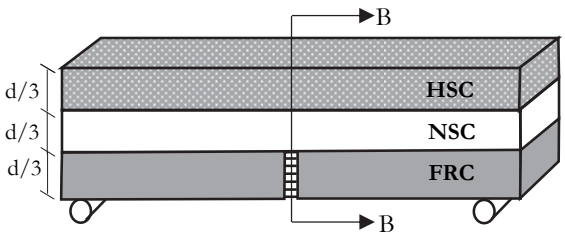

b) MC-FGC pattern

Cross section: B-B

Figure 1:Patterns of FRC and FGC beams and the SF distributions across the notch.

Experimental test setup

Hillerborg[25]recommended standard 3PB notched beams to calculate the fracture toughness of concrete. 3PB specimens were employed in the TPFM proposed by Jenq and Shah [21,24], which this model was adopted in the present work to analyze the results of the matrix cracked specimens. Therefore, the FGC and FD FRC beams were tested under the 3PB test. A universal testing machine of 1000 kN maximum capacity was used for testing all specimens. Flexural test measurements were obtained through a data acquisition system. A100 kN maximum capacity load cell was used to measure the applied load. The crack mouth opening displacement (CMOD) was measured using a sensitive LVDT, as shown schematically in Fig. 3. However, the CTOD was measured based on the proposed relationships of ETPFM.

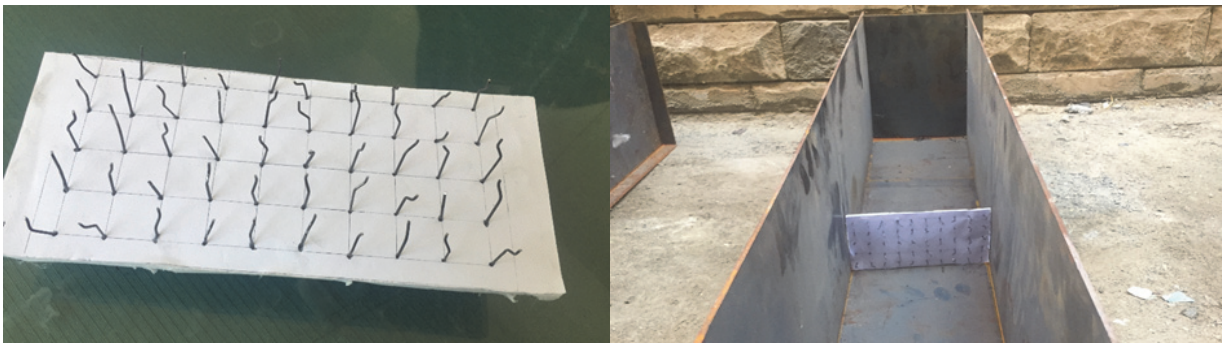

Figure 2: Methodology of MC-FD FRC and FGC beams.

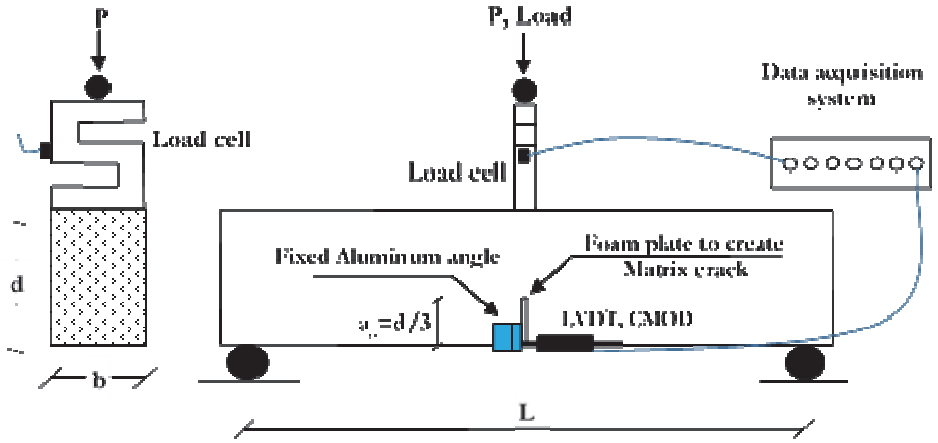

Figure 3: Schematic diagram for setting CMOD measurement and test set up.

Equivalent parameters of TPFM method (ETPFM)

The flexural strength f_{fl} was calculated using a three-point bending test (3PB) for different specimens sizes as follow;

$$f_{fl} = \frac{My}{I} = \frac{3PL}{2bd^2} \tag{1}$$

Where M is the moment due to the applied load, P, under 3PB test, y is the maximum distance from the neutral axis of specimen cross-section, I is the moment of inertia for uncracked specimen, b is the specimen breadth, d is the depth and L is the loaded span of the specimen. It is worth noting that since there is no alternative for Eqn. (1), this equation can be used for composite comparison data and specification values up to the maximum fiber strain of 2 % and considered an apparent strength for laminated beams as recommended by ASTM D7264/D7264M [39].

Ouyan et al.[26]proposed a relationship based on equivalency between the effective crack growth length (Δa_e) of TFPM proposed by Jenq and Shah [21]and critical crack length of SEL (C_f)[22]. The relations of ETPFM were suggested to predicate the fracture parameters (K_{IC}, $CTOD_C$) for infinity large size 3B.P beam without using a closed-loop of loading and unloading cycle as in TFPM, by the following equations;

$$G_f = \frac{1.261\ \pi\ \sigma_f^2 \left(a_0 + c_f\right)}{E} \tag{2}$$

$$K_{IC} = \sqrt{G_f E} \tag{3}$$

$$CMOD_c = \frac{4.68\ \sigma_f (a_0 + c_f)}{E} \tag{4}$$

$$CTOD_c = CMOD_c \left[1 - 0.92\left(\frac{a_0}{a_0 + c_f}\right) - 0.08\left(\frac{a_0}{a_0 + c_f}\right)^2\right] \tag{5}$$

$$CTOD_c = 2.854\sqrt{\frac{G_f}{E}\left(0.081a_0 + c_f - \frac{0.081a_0^2}{a_0 + c_f}\right)} \tag{6}$$

Where σ_f is the nominal strength and expressed by f_{fl} for MC-specimen, a_o is the initial pre-crack depth, G_f is the critical energy release rate, C_f is the effective crack length, E is the modulus of elasticity, and CTODc is the critical crack

mouth displacement. Also, modulus of elasticity can be obtained from the load-CMOD curve for notched for FD FRC specimens as follow[2,21,24]:

$$E = \frac{6\,L\,a_0\,V(\alpha)}{C_i\,d^2\,b} \tag{7}$$

$$V(\alpha) = 0.76 - 2.28\alpha + 3.87\alpha^2 - 2.04\alpha^3 + \frac{0.66}{(1-\alpha)^2} \tag{8}$$

Ci is the initial compliance calculated from the load-CMOD curve, and V(α) is the geometry factor.
It is worth noting that the apparent flexural modulus of orthotropic laminates can be calculated by the Chord or Secant method recommended by ASTM D7264/D7264M [39]. On the other hand, Eqns. (7,8) were previously adopted to estimate the modulus of elasticity of FRC [21,24]and FGC [2]. Therefore, the modulus of elasticity was calculated for FRC and FGC specimens using Eqns. (7,8).
Eqn. (7) calculated the modulus of elasticity for FD FRC as an apparent value to the whole composite layered FGC beams. To calculate a representative E, especially for FGC specimens, notched FGC specimens with relative notch depth (α_o=1/6) were tested for this study, as the FD of bottom layer for MC-FGC with α_o=1/3 was fully cracked.

Results and Discussion

Flexural behavior of MC-specimens

The results of flexural strength for MC-FD FRC, and MC-FGC specimens at first crack initiation and maximum stress for specimens with different sizes and L/d ratios equal 4, 5, and 6 are given in Tab. 2.

Specimens			MC-FD FRC		MC-FGC
Beam Code	L/d ratio	b×d×L, mm	f_{fl} at first cracking, MPa	f_{fl} at Maximum stress, MPa	f_{fl} at Maximum stress, MPa
B4-1	4	150×150×600	3.17	3.70	2.75
B4-2	4	150×187.5×750	2.79	3.78	3.18
B4-3	4	150×225×900	2.60	3.23	2.58
B5-1	5	150×150×750	2.57	3.34	3.04
B5-2	5	150×180×900	2.90	3.34	2.65
B6	6	150×150×900	2.74	2.84	2.62
E, GPa			27.00		33.30

Table 2: Results of flexural strength of MC-FD FRC and FGC specimens.

Fig. 4 shows stress-CMOD curves of MC-FD FRC and MC-FGC specimens with different sizes and span- depth ratios equal four, five, and six. The regulation factor was calculated for the tested specimens according to the suggested multi-linear mean curve. The suggested multi-linear mean curve was calculated based on average points of stress and CMOD at each observed variation on the curve slope for the four specimens in each case. For clear observation of the points at first cracking and maximum stress, the mean curves of MC-FD FRC and MC-FGC specimens were re-drawn up to CMOD equals 5 mm, as shown in Fig. 5.

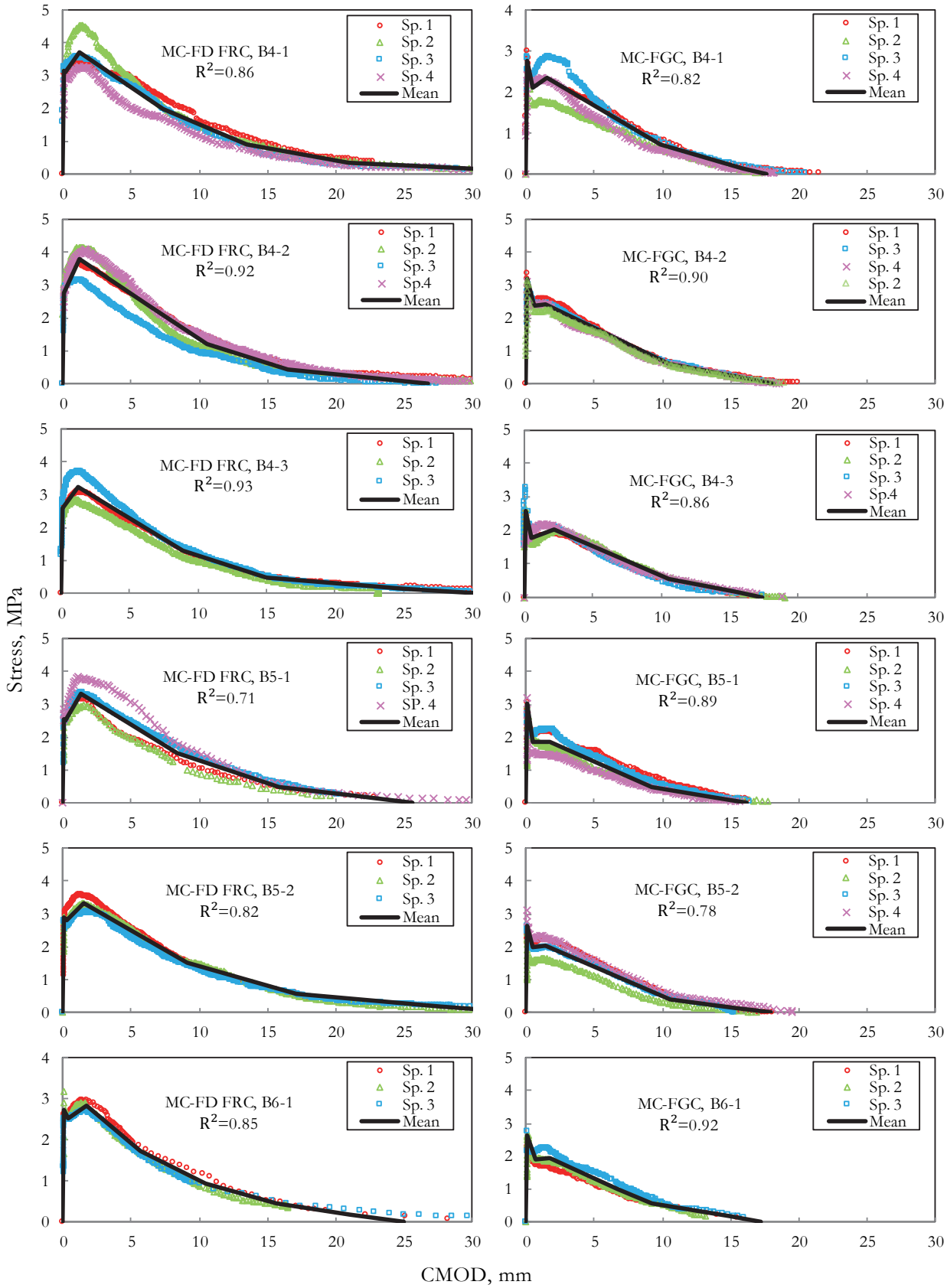

a) MC-FD FRC beams b) MC-FGC beams

Figure 4: Stress-CMOD curves of MC-beams, (a) FRC, and (b) FGC.

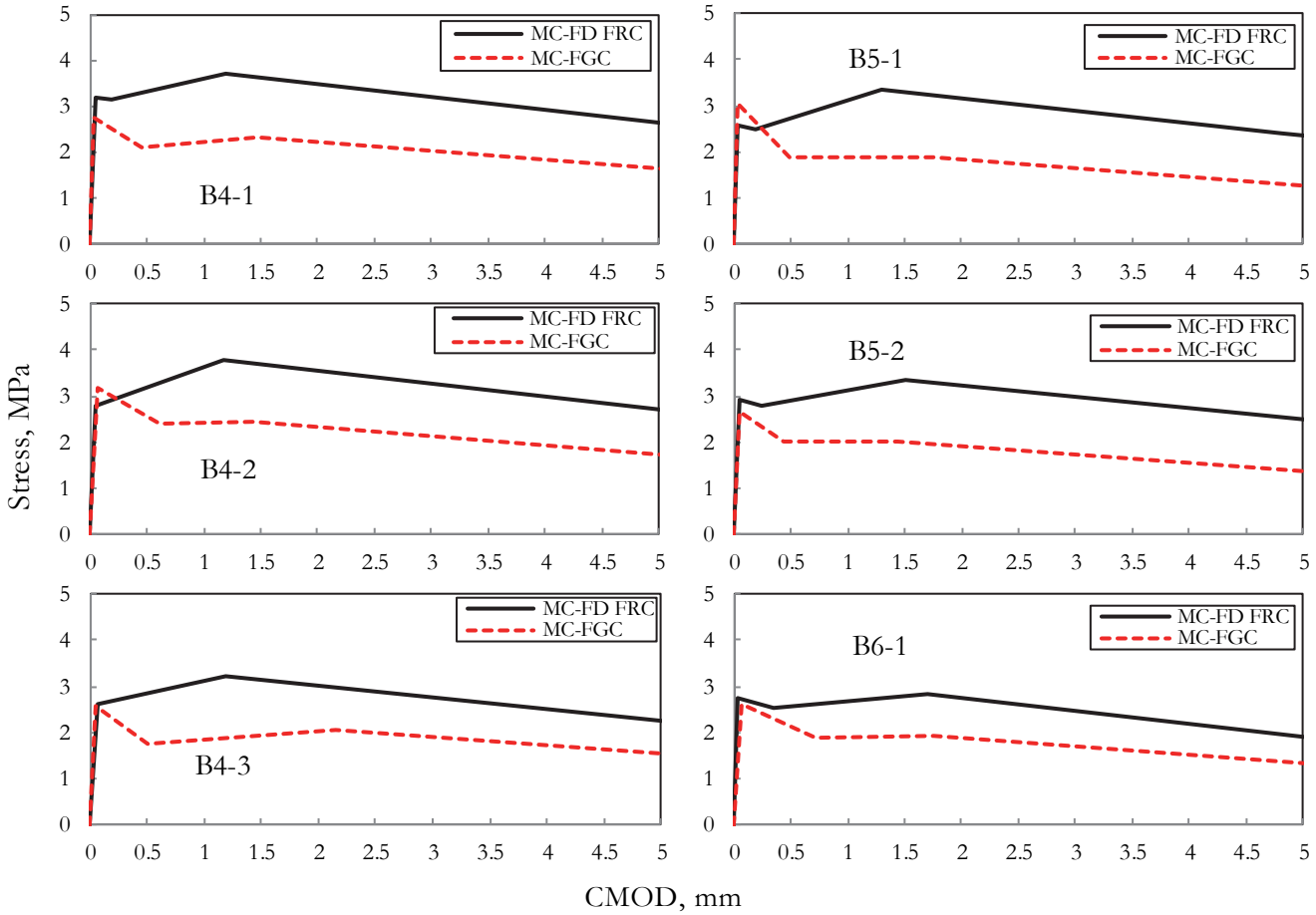

Figure 5: Mean curves of Stress-CMOD for MC- FD FRC and MC-FGC beams.

For MC-FD FRC specimens, the first crack initiation appeared before the maximum stress, and specimens showed strain hardening behavior as a result of SFs at the head of the crack tip. The stress is released slowly after that depending on fibers distribution through the beam cross-section. While in MC- FGC, the first crack initiation occurred at maximum stress, and an abrupt fall was seen after the maximum stress in MC- FGC specimens as a result of the SFs absence ahead of the crack tip, see Fig. 1. These observations of crack initiation for FRC specimens are compatible with ACI 544.4R-88 and ASTM C1609/C1609M [40,41]. On the other hand, the area under the descending portion (softening portion) of the FRC specimens is larger than that of the FGC specimens. This is due to SFs in the FD FRC beam specimens. Also, in MC-FGC specimens, the concrete layers ahead of the crack tip were NSC in the middle zone and HSC in the compression zone without SF. Thus, the presence of the softening portion in the FGC specimens reflects the efficiency of the proposed new MC technique in simulating a real field crack in the laboratory.

Results of ETPFM

According to Ouyang et al. [26], the fracture parameters (K_{IC}, CTODc) can be obtained from the suggested equivalency relationship (ETPFM), based on the equivalency of the effective crack length of TPFM and SEL. The effective crack lengths (C_f) for MC-FRC and MC –FGC specimens were obtained from applying SEL-Type II on the specimens B4-1, B4-2, and B4-3, with a constant L/d ratio, equals 4. These values were considered as constant material property. The values of C_f were 1.82, 14.27, and 63.43 mm for MC-FD FRC at first cracking, MC-FD FRC, and MC-FGC at maximum stress, respectively. According to Bažant and RILEM recommendations [42], the boundary of the cracking layer size, fracture process zone (FPZ), is approximate twice C_f. Thus, the statistical analysis to obtain the equivalent parameters from ETPFM was adopted within the boundary of the FPZ. The proposed ETPFM relationships were applied on MC-FD FRC and MC-FGC specimens with α_0 equal 1/3, for each case of L/d ratios (4, 5, and 6) individually, at first cracking and maximum stress, as follows:

The values of G_f and K_{IC} were estimated for the four specimens representing each case of L/d individually by substituting the incremental increase steps value of C_f in Eqn. (2,3). The CTOD at each incremental step of C_f is obtained from Eqns. (4,5). Then, K_{IC}-CTOD curves for specimens with L/d ratios equal 4, 5, 6, and their average curves can be drawn as shown in Figs. 6, 7, 8(a), for each case individually. By estimating the standard deviation (S.D) for the average values of CTOD at each incremental step, the average CTOD with minimum standard deviation is considered as a material parameter ($CTODc^S$), as shown in Fig. 6, 7, 8(b). The second fracture parameter, K_{IC}^S, was calculated by substituting $CTODc^S$ into K_{IC} –CTOD's average curve, see Figs. 6, 7, 8(a). In addition, the effective crack length, C_f^S, proposed by ETPFM relationship at different notch lengths can be obtained from Eqn. (6).

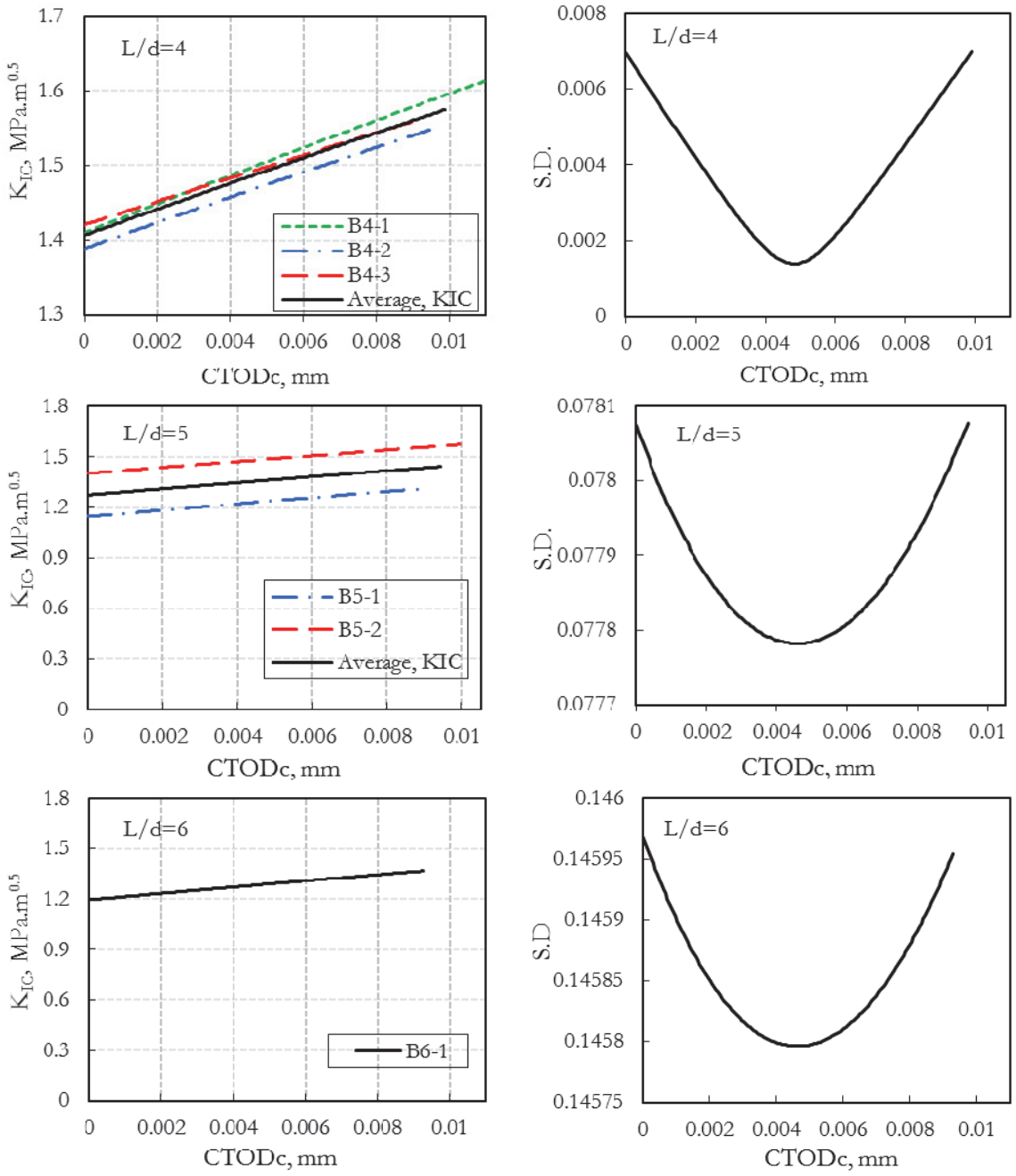

a)K_{IC}-CTODc curves b)Relationship between S.D. and CTODc

Figure 6: MC-FD FRC at first cracking at different L/d ratios equals 4, 5 and 6.

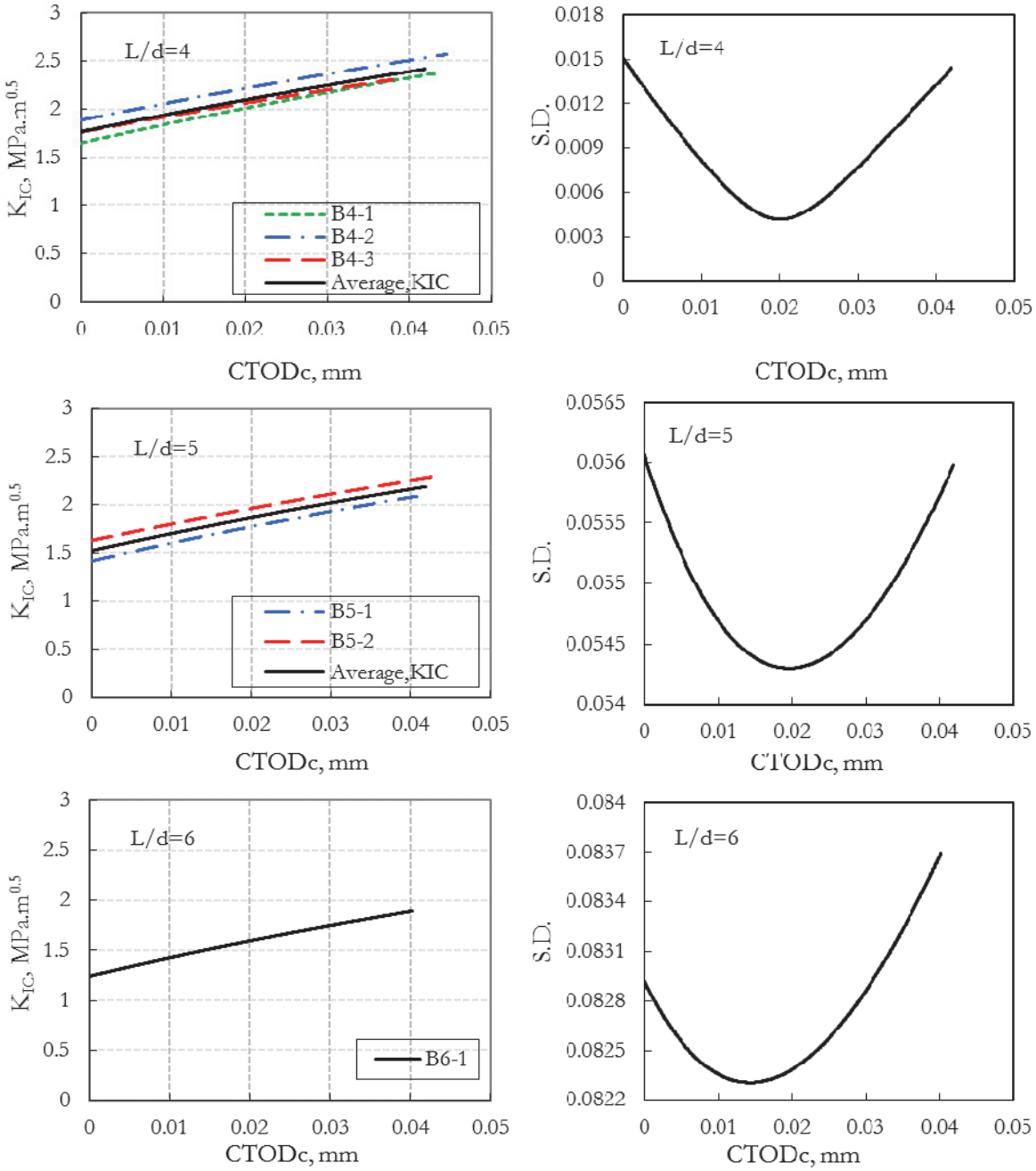

a)K_{IC}-CTODc curves b)Relationship between S.D. and CTODc

Figure 7: MC-FD FRC at max stress at different L/d ratios equals 4, 5 and 6.

Tab. 3 shows the proposed parameters of ETPFM for MC-FD FRC and MC-FGC at first cracking and maximum stress. It is clear that K_{IC}^{S} values for MC-FRC and MC-FGC showed an inversely proportional to L/d ratios, as known. Ouyang et al. [26] calculated the fracture properties of NSC by its suggested method, equivalent TPFM, based on experimental results of Bažant and Pfeiffer [43]and showed agreement with the results of SEL. Four different beams with a constant L/d ratio equal to 2.50, f_{cu}=33.5MPa, and E= 27.7GPa were investigated. The results of ETPFM parameters of NSC were K_{IC}=0.99 MPa.m$^{0.5,}$ and C_f =11.12 mm. As known, the K_{IC} values are inversely proportional to L/d ratios, so

the K_{IC} value for NSC is expected to be higher than its value for specimens with an L/d ratio equal to four. Comparing NSC results with MC-FD FRC at first cracking and maximum stress for specimens with an L/d ratio equal to 4, variance in concrete size can be neglected.

On the other hand, the presence of fibers ahead and behind the crack tip of the MC specimen significantly affects K_{IC}. Undoubtedly, this significant increase is due to the bridging and the closing effects of SFs. This also refutes the assumptions of equality of K_{IC} for NSC and FRC at first cracking. Thus, the actual fracture toughness of MC beams is recommended to calculate the fracture toughness of FD FRC and FGC.

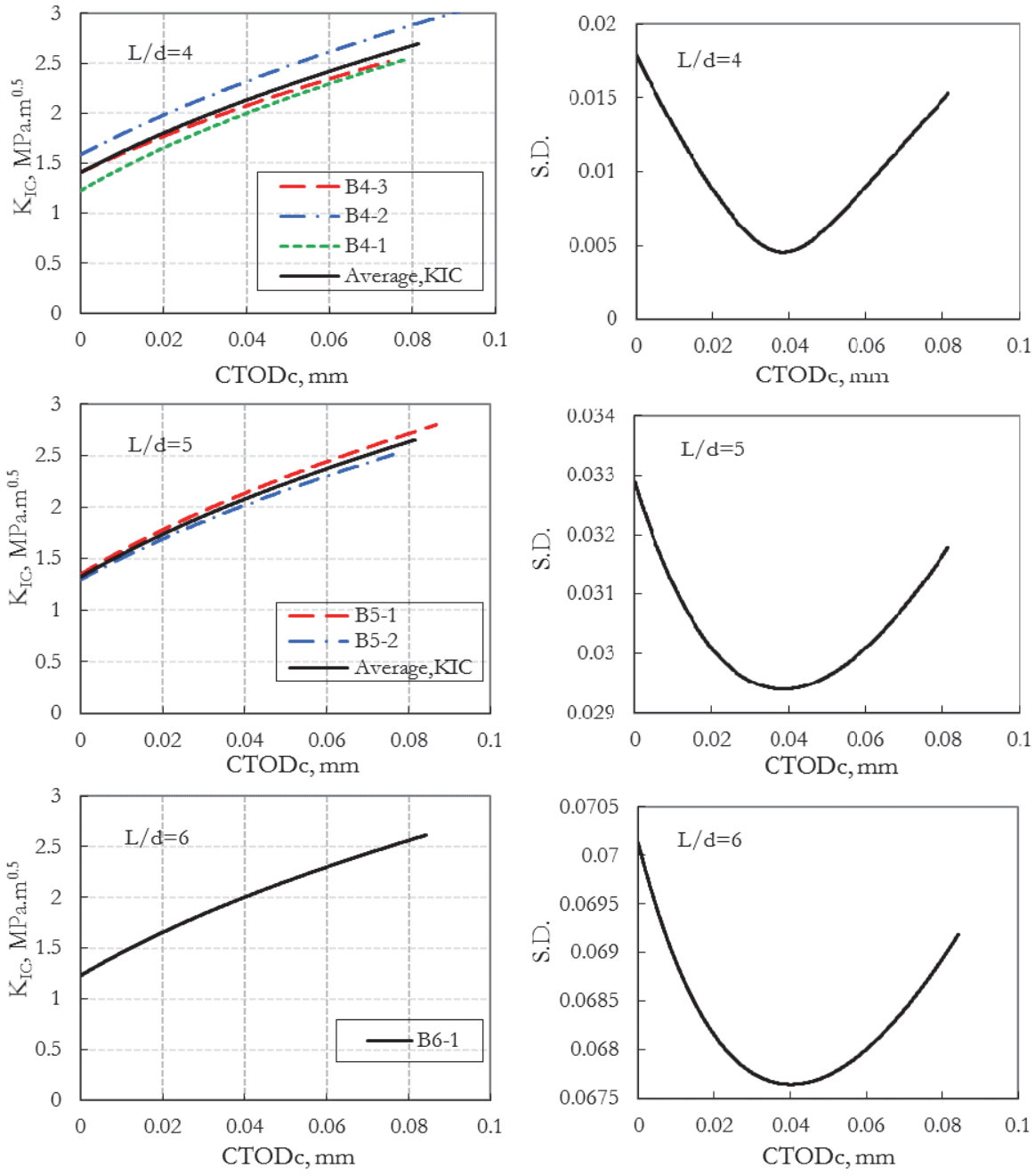

a)K_{IC}-CTODc curves b)Relationship between S.D. and CTODc

Figure 8: MC-FGC at max stress at different L/d ratios equals 4, 5 and 6.

Beam Code	L/d	MC-FD FRC			MC-FD FRC			MC-FGC		
		at first cracking			at max stress			at max stress		
		K_{IC}^S, MPa.m$^{0.5}$	$CTOD_C^S$, mm	C_f^S, mm	K_{IC}^S, MPa.m$^{0.5}$	$CTOD_C^S$, mm	C_f^S, mm	K_{IC}^S, MPa.m$^{0.5}$	$CTOD_C^S$, mm	C_f^S, mm
B4-1				0.888			7.70			43.3
B4-2	4	1.49	0.0048	0.892	2.09	0.20	7.695	2.10	0.038	43.1
B4-3				0.897			7.69			43.0
B5-1				0.972			9.373			46.10
B5-2	5	1.36	0.0046	0.975	1.86	0.196	9.361	2.05	0.039	45.90
B6	6	1.28	0.00464	1.108	1.50	0.0143	7.668	2.00	0.040	52.7

Table 3: The proposed parameters of ETPFM for MC-FD FRC and MC-FGC.

Reliability of the present predicted fracture toughness

Reliability of the predicted K_{IC} from ETPFM for MC-FD FRCwas examined, at first cracking and maximum stress, with L/d ratios equal to 4, 5, and 6. The concept of the maximum size of the non-damaged defect (d_{max}) was used in this study [30,31,44–47]. It is based on the concept of critical distance theory and has an obvious indication of the maximum imperfection size present in a material. Pook[48,49] used this theory to calculate the maximum size of imperfection in metals subjected to repeated loads. Alternatively, d_{max} it is analogous to the characteristic length $(l_{ch} = \frac{EG_F}{f_t^2})$[49–51]. Thus, d_{max} is equal to $\frac{1}{\pi}\left(\frac{K_{IC}}{1.12 \times f_{fl}}\right)^2$, where f_{fl} is the flexural strength for smooth specimens. The values of f_{fl} of smooth specimens were obtained from previous research by Sallam and co-workers [5]for the same dimensions of MC specimens. The consistency of K_{IC} has been examined by comparing the value of d_{max} with nominal maximum aggregate size (NMAZ). Logically, the values of d_{max} /NMAZ should be around unity. Sallam and co-workers found that for rigid pavement, the ratio d_{max} /NMAZ< 2 [31] and for flexible pavement, this ratio is less than 0.75 [46]. Fig. 9-a shows the d_{max} /NMAZ for MC-FDFRC at the first cracking range between 1.01 and 1.54. The values were considered close to unity. Also, the maximum damage of ETPFM was considered close to the NMAZ. Also, Fig. 9-b shows that d_{max} /NMAZ for MC-FD FRC at maximum stress range between 1.38and 2.89. The increase in d_{max} /NMAZ ratios is considered appropriate at maximum stress, as the damage is larger than at first cracking.

In the case of through-thickness crack, d_{max} /NMAZ was found to be less than unity [30,31]. A similar finding was found in the present work for MC-FD FRC at first cracking with a small increase due to fibers' closing effect in MC. The discrepancy and the higher values of MC-FD FRC at maximumstresscompared to [30,31]can be attributed to the bridging and closing effect of short steel fibers, which subsequently increases the ratio between the fracture toughness and the smooth specimen flexural strength. These findings indicate that K_{IC} value for MC-specimens predicted from ETPFM is considered appropriate according to d_{max} concept.

Comparison between experimental and predicted results from ETPFM

Another effective method to examine the reliability of ETPFM methods is by comparing the expected results of $CMOD_C$ predicted from this method by the present experimental results at first crack initiation. Due to the direct proportionality between K_{IC} and the characteristic crack length according to each method, the predicted $CMOD_C$ can be calculated based on the predicted effective crack growth extension (C_f^SorΔa_e) and critical flexural strength. Thus, the proposed equation to predict $CMOD_C$ by C_f values calculated from ETPFM is Eqn. (4), see Tab. 3. Fig. 10 shows the predicted $CMOD_C^S$ values from ETPFM and the experimental values of stress-$CMOD_C$, Fig. 5, for all specimens with different L/d ratios equal to 4, 5, and 6 at first cracking for MC-FD FRC and MC-FGC. All values of the experimental and predicted results of

$CMOD_C$were in the range of 0.028 to 0.06 mm, and 0.038 to 0.071 mm for MC FD FRC and MC-FGC, respectively. The percentage error between the predicted and the experimental CMOD was calculated for all FD-FRC and FGC beams, and the results are given in Tab. 4. The mean % error for all beams of FD-FRC and FGC were -27% and 24.8%, respectively.

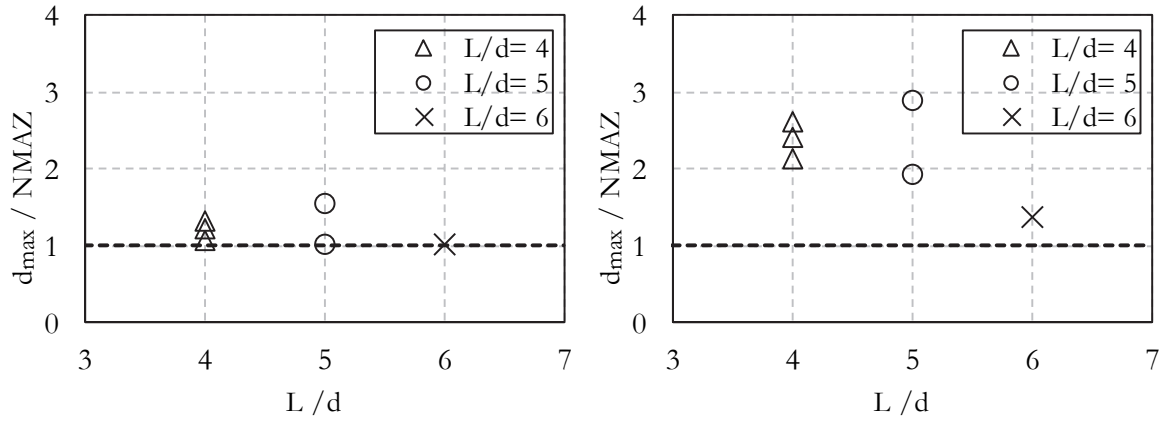

a) MC-FD FRC at first cracking b) MC-FRC at max stress

Figure 9:The fracture toughness reliability for MC-FD FRC was measured based on E-TPFM at different L/d ratios.

Beam Code	L/d	MC-FD FRC			MC-FGC		
		Experimental CMOD, mm	Predicted $CMOD_C^S$, mm	% Erorr	Experimental CMOD, mm	Predicted $CMOD_C^S$, mm	% Erorr
B4-1		0.045	0.034	-24	0.038	0.054	42
B4-2	4	0.052	0.037	-29	0.06	0.071	18
B4-3		0.06	0.042	-30	0.05	0.064	28
B5-1	5	0.04	0.028	-30	0.038	0.059	55
B5-2		0.045	0.037	-18	0.05	0.058	16
B6	6	0.041	0.029	-29	0.06	0.054	-10

Table 4: The Experimental and predicted values of $CMOD_C$ at first cracking with the % error for MC-FD FRC and MC-FGC.

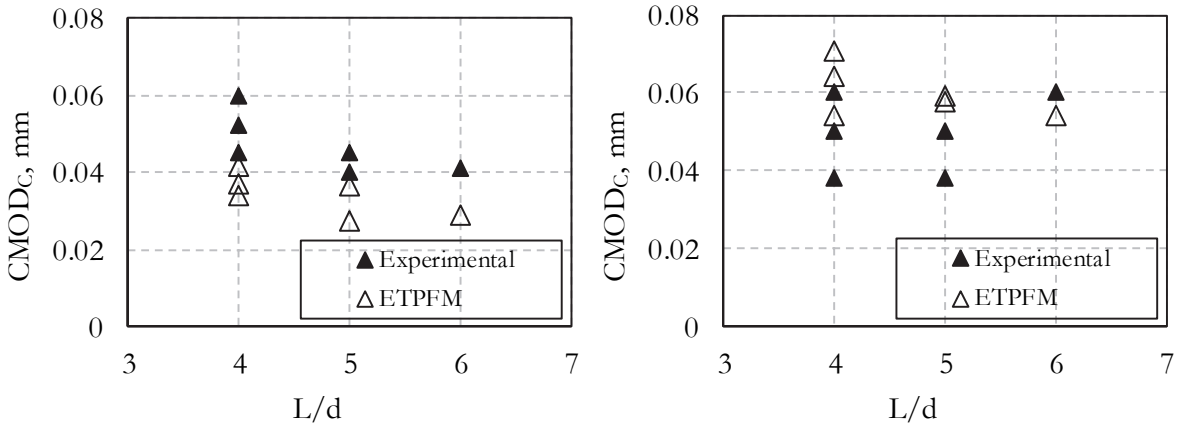

a) MC- FD FRC at first cracking b) MC-FGC at max stress

Figure 10:Comparison between results of $CMOD_C$ from experimental by the predicted from ETPFM.

CONCLUSION

The results of the present work support the following conclusions:

1. In the case of MC-FD FRC beams, the first crack initiation appeared before the maximum stress due to the presence of SFs ahead of the crack tip. However, the first crack initiation occurred at the maximum stress of MC- FGC beams due to the absence of SFs ahead of the crack tip.
2. The presence of the softening portion in FGC beam specimens reflects the efficiency of the proposed new matrix crack technique in simulating a real field crack in the laboratory. Thus, the actual fracture toughness of FRC beams is recommended to be calculated by real matrix crack, not through-thickness cracked specimens.
3. The predicted values of K_{IC} for matrix crack specimens estimated by ETPFM are considered appropriate according to the maximum size of the non-damaged defect d_{max} concept.
4. The $CMOD_C$ estimated from ETPFM were in the range of 0.028-0.06 mm with a mean % error of 27 % and 0.038-0.071 mm with a mean % error of 24.8 %, respectively for all MC FD FRC and MC-FGM beams.

REFERENCES

[1] ACI 544.4R-18. (2018). Guide for design with fiber-reinforced concrete, Am. Concr. Inst., pp. 1–33.

[2] Roesler, J., Paulino, G., Gaedicke, C., Bordelon, A., Park, K. (2007). Fracture behavior of functionally graded concrete materials for rigid pavements, J. Transp. Res. Board Natl. Acad. Washington., (2037), pp. 40–49, DOI: 10.3141/2037-04.

[3] Dias, C.M.R., Savastano, H., John, V.M. (2010). Exploring the potential of functionally graded materials concept for the development of fiber cement, Constr. Build. Mater., 24(2), pp. 140–146, DOI: 10.1016/j.conbuildmat.2008.01.017.

[4] ACI 544.1R-96. (2009). Report on fiber reinforced concrete, ACI Man. Concr. Pract.

[5] Elakhras, A.A., Seleem, M.H., Sallam, H.E.M. (2021). Intrinsic fracture toughness of fiber reinforced and functionally graded concretes: an innovative approach, Eng. Fract. Mech., 258, DOI: 10.1016/j.engfracmech.2021.108098.

[6] Iskhakov, I., Ribakov, Y., Holschemacher, K., Mueller, T. (2013). High performance repairing of reinforced concrete structures, Mater. Des., 44, pp. 216–222, DOI: 10.1016/j.matdes.2012.07.041.

[7] Iskhakov, I., Ribakov, Y. (2013). A new concept for design of fibered high strength reinforced concrete elements using ultimate limit state method, Mater. Des., 51, pp. 612–619, DOI: 10.1016/j.matdes.2013.04.063.

[8] Naghibdehi, M.G., Mastali, M., Sharbatdar, M.K., Naghibdehi, M.G. (2014). Flexural performance of functionally graded RC cross-section with steel and PP fibres, Mag. Concr. Res., 66(5), pp. 219–233, DOI: 10.1680/macr.13.00248.

[9] Naghibdehi, M.G., Naghipour, M., Rabiee, M. (2015). Behaviour of functionally graded reinforced- concrete beams under cyclic loading, Gradjevinar, 67(5), pp. 427–439, DOI: 10.14256/JCE.1124.2014.

[10] Chan, R., Liu, X., Galobardes, I. (2020). Parametric study of functionally graded concretes incorporating steel fibres and recycled aggregates, Constr. Build. Mater., 242, DOI: 10.1016/j.conbuildmat.2020.118186.

[11] Prasad, N., Murali, G. (2021). Research on flexure and impact performance of functionally-graded two-stage fibrous concrete beams of different sizes, Constr. Build. Mater., 288, DOI: 10.1016/j.conbuildmat.2021.123138.

[12] Prasad, N., Murali, G. (2021). Exploring the impact performance of functionally-graded preplaced aggregate concrete incorporating steel and polypropylene fibres, J. Build. Eng., 35, DOI: 10.1016/j.jobe.2020.102077.

[13] Mastali, M., Naghibdehi, M.G., Naghipour, M., Rabiee, S.M. (2015). Experimental assessment of functionally graded reinforced concrete (FGRC) slabs under drop weight and projectile impacts, Constr. Build. Mater., 95, pp. 296–311, DOI: 10.1016/j.conbuildmat.2015.07.153.

[14] Amparano, F.E., Xi, Y., Roh, Y.S. (2000). Experimental study on the effect of aggregate content on fracture behavior of concrete, Eng. Fract. Mech., 67(1), pp. 65–84, DOI: 10.1016/S0013-7944(00)00036-9.

[15] Xu, W., Chen, B., Chen, X., Chen, C. (2021). Influence of aggregate size and notch depth ratio on fracture performance of steel slag pervious concrete, Constr. Build. Mater., 273, pp. 122036, DOI: 10.1016/j.conbuildmat.2020.122036.

[16] Zhao, Z., Kwon, S.H., Shah, S.P. (2008). Effect of specimen size on fracture energy and softening curve of concrete: Part I. Experiments and fracture energy, Cem. Concr. Res., 38(8–9), pp. 1049–1060, DOI: 10.1016/j.cemconres.2008.03.017.

[17] Bažant, Z.P., Rasoolinejad, M., Dönmez, A., Luo, W. (2019). Dependence of fracture size effect and projectile penetration on fiber content of FRC, IOP Conf. Ser. Mater. Sci. Eng., 596(1),

DOI: 10.1088/1757-899X/596/1/012001.
[18] Bažant, Z.P., Yu, Q., Zi, G. (2002). Choice of standard fracture test for concrete and its statistical evaluation, Int. J. Fract., 118(4), pp. 303–337, DOI: 10.1023/A.
[19] Hillerborg, A., Modéer, M., Petersson, P.E. (1976). Analysis of crack formation and crack growth in concrete by means of fracture mechanics and finite elements, Cem. Concr. Res., 6(6), pp. 773–781, DOI: 10.1016/0008-8846(76)90007-7.
[20] Bažant, Z.P., Oh, B.H. (1983). Crack band theory for fracture of concrete, Mater. Struct., 16(May), pp. 155–177, DOI: 10.1007/BF02486267.
[21] Jenq, Y.S., Shah, S.P. (1985). A fracture toughness criterion for concrete, Eng. Fract. Mech., 21(5), pp. 1055–1069, DOI: 10.1016/0013-7944(85)90009-8.
[22] Bažant, Z.P., Yu, Q. (2009). Universal size effect law and effect of crack depth on quasi-brittle structure strength, J. Eng. Mech., 135(2), pp. 78–84, DOI: 10.1061/(ASCE)0733-9399(2009)135:2(78).
[23] Han, X., Chen, Y., Xiao, Q., Cui, K., Chen, Q., Li, C., Qiu, Z. (2021). Determination of concrete strength and toughness from notched 3 PB specimens of same depth but various span-depth ratios, Eng. Fract. Mech., 245, DOI: 10.1016/j.engfracmech.2021.107589.
[24] Jenq, Y.S., Shah, S.P. (1986). Crack propagation in fiber reinforced concrete, J. Struct. Eng. Am. Soc. Civ. Eng., 112(1), pp. 19–34.
[25] Hillerborg, A. (1985). The theoretical basis of a method to determine the fracture energy Gf of concrete, Mater. Struct., 18(106), pp. 291–296.
[26] Ouyang, C., Tang, T., Shah, S.P. (1996). Relationship between fracture parameters from two parameter fracture model and from size effect model, Mater. Struct., 29(2), pp. 79–86, DOI: 10.1007/bf02486197.
[27] Park, K., Paulino, G.H., Roesler, J. (2010). Cohesive fracture model for functionally graded fiber reinforced concrete, Cem. Concr. Res., 40(6), pp. 956–965, DOI: 10.1016/j.cemconres.2010.02.004.
[28] Nazari, A., Sanjayan, J.G. (2015). Stress intensity factor against fracture toughness in functionally graded geopolymers, Arch. Civ. Mech. Eng., , pp. 1–10, DOI: 10.1016/j.acme.2015.06.005.
[29] El-Sagheer, I., Abd-Elhady, A.A., Sallam, H.E.D.M., Naga, S.A.R. (2021). An assessment of ASTM E1922 for measuring the translaminar fracture toughness of laminated polymer matrix composite materials, Polymers (Basel)., 13(18), DOI: 10.3390/polym13183129.
[30] Al Hazmi, H.S.J., Al Hazmi, W.H., Shubaili, M.A., Sallam, H.E.M. (2012). Fracture energy of hybrid polypropylene-steel fiber high strength concrete, WIT Trans. Built Environ., 124, pp. 309–318, DOI: 10.2495/HPSM120271.
[31] Sallam, H.E.D.M., Mubaraki, M., Yusoff, N.I.M. (2014). Application of the maximum undamaged defect size (dmax) concept in fiber-reinforced concrete pavements, Arab. J. Sci. Eng., 39(12), pp. 8499–8506, DOI: 10.1007/s13369-014-1400-4.
[32] ACI 211.1-91. (2009). Standard practice for selecting proportions for normal, heavyweight, and mass concrete, Am. Concr. Inst., (Reapproved 2009), pp. 1–38.
[33] BS EN 12390-3:2019. (2019). Testing hardened concrete- Compressive strength of test specimens, BSI Stand. Publ. London.
[34] BS EN 12390-6:2009. (2009). Testing hardened concrete - Tensile splitting strength of test specimens, BSI Stand. Publ. London.
[35] Othman, M.A., El-Emam, H.M., Seleem, M.H., Sallam, H.E.M., Moawad, M. (2021). Flexural behavior of functionally graded concrete beams with different patterns, Arch. Civ. Mech. Eng., 21(4), DOI: 10.1007/s43452-021-00317-0.
[36] Dupont, D., Vandewalle, L. (2005). Distribution of steel fibres in rectangular sections, Cem. Concr. Compos. 27, pp. 391–398, DOI: 10.1016/j.cemconcomp.2004.03.005.
[37] Kazemi, M.T., Golsorkhtabar, H., Beygi, M.H.A.A., Gholamitabar, M. (2017). Fracture properties of steel fiber reinforced high strength concrete using work of fracture and size effect methods, Constr. Build. Mater., 142, pp. 482–489, DOI: 10.1016/j.conbuildmat.2017.03.089.
[38] Ahmad, I., Qing, L., Khan, S., Cao, G., Ijaz, N., Mu, R. (2021). Experimental investigations on fracture parameters of random and aligned steel fiber reinforced cementitious composites, Constr. Build. Mater., 284, DOI: 10.1016/j.conbuildmat.2021.122680.
[39] ASTM D7264/D7264M-15. (2015). Standard test method for flexural properties of Polymer Matrix Composite Materials, Annu. B. ASTM Stand., pp. 1–11, DOI: 10.1520/D7264_D7264M-15.
[40] ASTM C1609/C1609M-12. (2013). Standard test method for flexural performance of fiber-reinforced concrete (Using beam with third-point loading) 1, ASTM Stand., 12(C 1609/C 1609M-12), pp. 1–8, DOI: 10.1520/C1609.
[41] ACI 544.4R-88. (2009). Design considerations for steel fiber reinforced, ACI Man. Concr. Pract.

[42] RILEM TC QFS. (2004). Quasibrittle fracture scaling and size effect- Final report1, Mater. Struct. Constr., 37(272), pp. 547–568, DOI: 10.1617/14109.
[43] Bažant, Z.P., Pfeiffer, P.A. (1987). Determination of fracture energy by size effect and brittleness number, ACI Mater. J., pp. 463–480.
[44] Abou El-Mal, H.S.S., Sherbini, A.S., Sallam, H.E.M. (2015). Mode II fracture toughness of hybrid FRCs, Int. J. Concr. Struct. Mater., 9(4), pp. 475–486, DOI: 10.1007/s40069-015-0117-4.
[45] Mousa, S., Abd-Elhady, A.A., Kim, G.Y., Sallam, H.E.M. (2018). Fracture behavior of roll bonded Al-brass-Al multilayer composites-Concept of the maximum undamaged defect size (d max), Procedia Struct. Integr., 13(January 2019), pp. 686–693, DOI: 10.1016/j.prostr.2018.12.114.
[46] Mubaraki, M., S.A. Osman., H.E.M. Sallam. (2019). Effect of RAP content on flexural behavior and fracture toughness of flexible pavement, Lat. Am. J. Solids Struct., 16(3), pp. 1–15.
[47] Mubaraki, M., Sallam, H.E.M. (2020). Reliability study on fracture and fatigue behavior of pavement materials using SCB specimen, Int. J. Pavement Eng., 21(13), pp. 1563–1575, DOI: 10.1080/10298436.2018.1555332.
[48] Pook, L.P. (1975). Analysis and application of fatigue crack growth data, J. Strain Anal. Eng. Des., 4(10), pp. 242–250.
[49] Taylor, D. (2007). The theory of critical distances: A new perspective in fracture mechanics, Oxford, UK, Elsevier.
[50] RILEM Committee on Fracture Mechanics of Concrete-Test Methods (RILEM 50-FMC). (1985). Determination of the fracture energy of mortar and concrete by means of three-point bend test on notched beams, Mater. Struct., 18, pp. 285–290.
[51] Rosselló, C., Elices, M., Guinea, G.V. (2006). Fracture of model concrete: 2. Fracture energy and characteristic length, Cem. Concr. Res., (36), pp. 1345–1353.